# Appendix A

A.1 Spectra of α Cir

In May 1996, I observed α Cir using the coudé spectrograph on the 74-inch Telescope at Mt. Stromlo. During two weeks, 4900 spectra were obtained with a wavelength range of 6000–7000Å and with a resolution of about 1.5Å (see Chapters 5–6 for results based on these spectra).

The template spectrum is shown in Figures A.1 and A.2. The S/N in this spectrum is over 1000 per pixel, though the continuum level is only accurate to about 0.01 and is less accurate in the regions specified.

The medium-resolution spectra have very little real continuum especially redward of Hα. Therefore, Jaymie Matthews (private communication) suggested that blending could have a significant effect on the measurement of the Hα bisector in α Cir (see Section 6.3.2 for discussion). In March 1997, I took some high-resolution spectra of α Cir, using with the coudé echelle spectrograph on the 74-inch Telescope. In order to determine which metal lines could affect the Hα profile, I reduced the two orders including Hα. The dispersion was about 0.05Å/pixel with a resolution of about 0.2Å. Part of the spectrum is shown in Figure A.3. The identification of the twenty most significant features is given in Table A.1. Above a relative intensity of 0.8 in the Hα line (referring to the intensity in the reduced medium-resolution spectra), the features C, F, Q, S and T contain metal lines which affect the profile. Below 0.8, only one feature is identified with a metal line, feature O containing Fe I 6569.2Å (rest wavelength) and a telluric line. The centre of Hα was measured to be at 6562.5Å, giving a Doppler shift of $-14\,\mathrm{km\,s^{-1}}$ for α Cir.
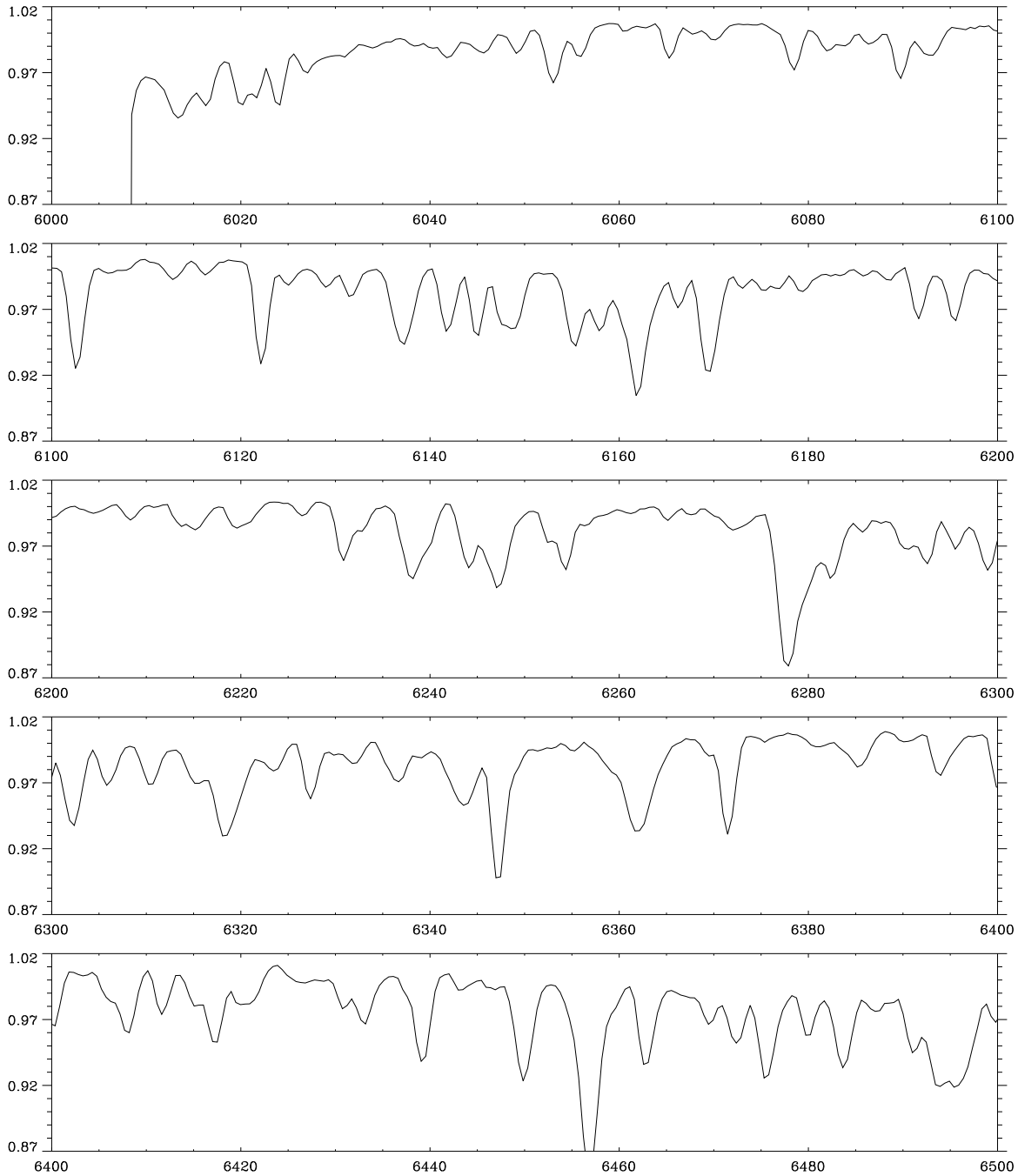
Figure A.1   Spectrum of α Cir from 6000 to 6500Å , taken with a medium resolution (~ 1.5Å)
spectrograph at Mt. Stromlo. Note that the continuum fit is not accurate below 6050Å.
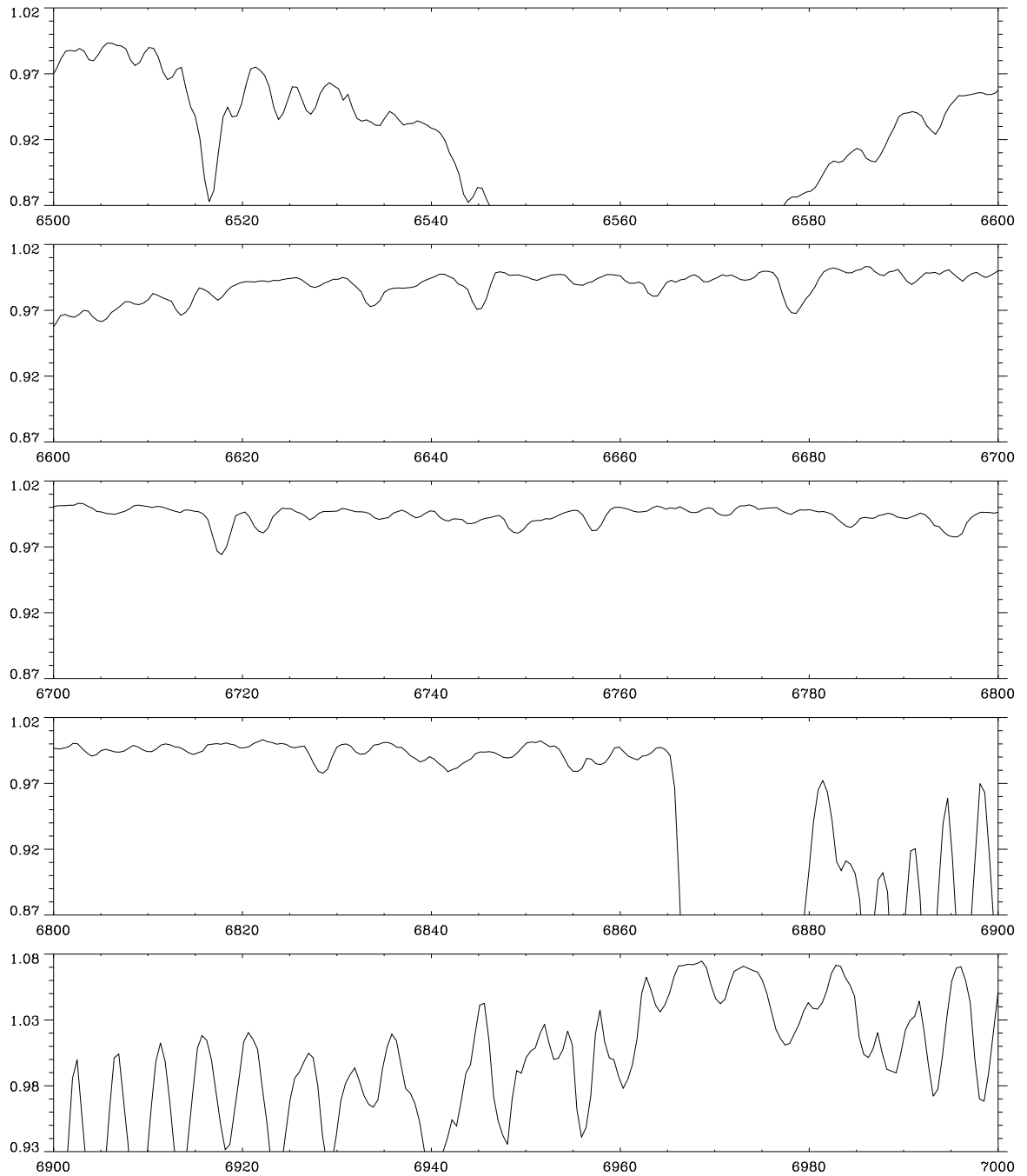
Figure A.2 Spectrum of α Cir from 6500 to 7000Å — continuation of Figure A.1. Note that the continuum fit is not accurate above 6900Å. The y-scale for this region is slightly shifted as a result.
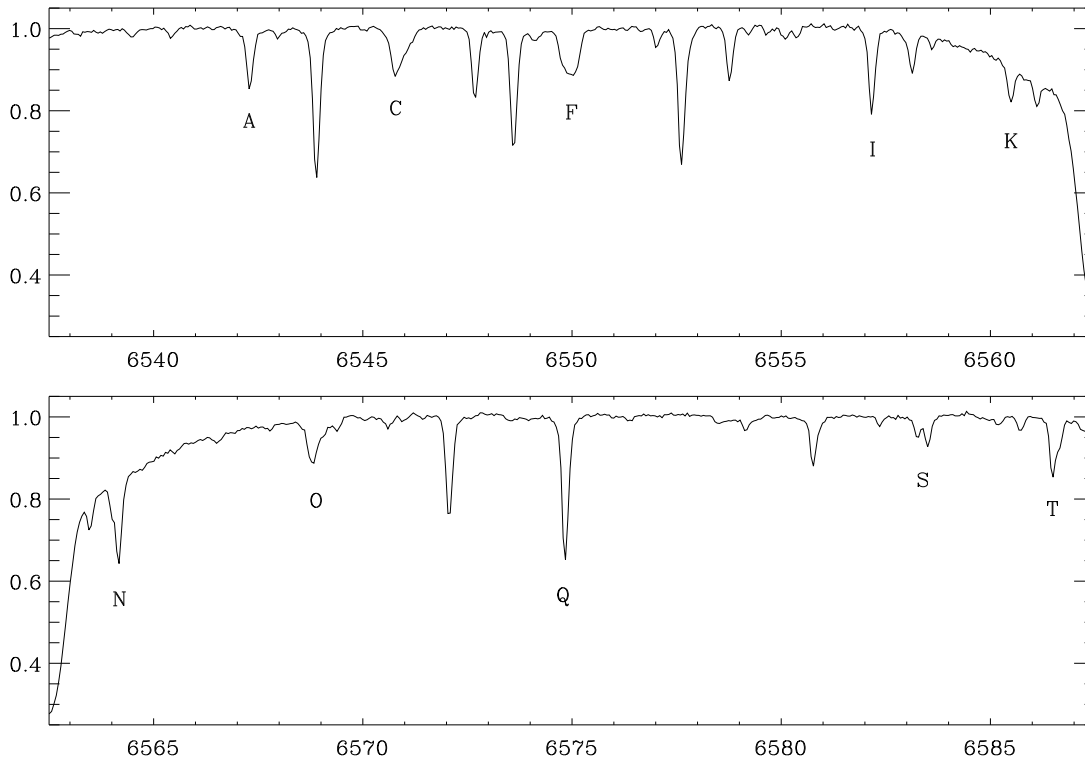
Figure A.3   Spectrum of α Cir within ± 25Å of the centre of Hα (6562.5Å), taken with a high resolution (~ 0.2Å) echelle spectrograph at Mt. Stromlo. The two panels are taken from different orders, with the intensity normalised by a fit made to the Hα wings below 6555 in the upper panel and above 6570 in the lower panel. Therefore, the intensities cannot be compared with the Hα line shown in other figures in this thesis, e.g. Figs. 6.1 and 6.3. This plot was used to identify the telluric and metal lines blending with Hα (see Section 6.3.2 and Table A.1). The letters A–T refer to the features in the Table.

Table A.1 Identification of absorption lines within the Hα profile of α Cir. For the twenty most significant features from the high resolution spectrum shown in Fig. A.3, the metal lines were identified using the synthetic spectrum calculated by Friedrich Kupka (private communication) and the telluric lines were identified using an atlas of the solar spectrum (Moore et al. 1966). Note that rest wavelengths are quoted and that the stellar spectrum of α Cir is shifted by about −0.3Å in this wavelength region.

feature	main line	other line
A	telluric 6542.31	
B	telluric 6543.91	
C	Fe I 6546.24	Mg II 6545.99
D	telluric 6547.70	
E	telluric 6548.62	
F	Sr I 6550.24	telluric 6550.28
G	telluric 6552.63	
H	telluric 6553.78	
I	telluric 6557.17	
J	telluric 6558.15	
K	telluric 6560.55	
L	telluric 6561.10	
M	telluric 6563.52	
N	telluric 6564.21	
O	Fe I 6569.22	telluric 6568.81
P	telluric 6572.09	
Q	telluric 6574.85	Fe I 6575.02
R	telluric 6580.78	
S	Si I 6583.71	telluric 6583.26
T	Fe II 6586.70	telluric 6586.51

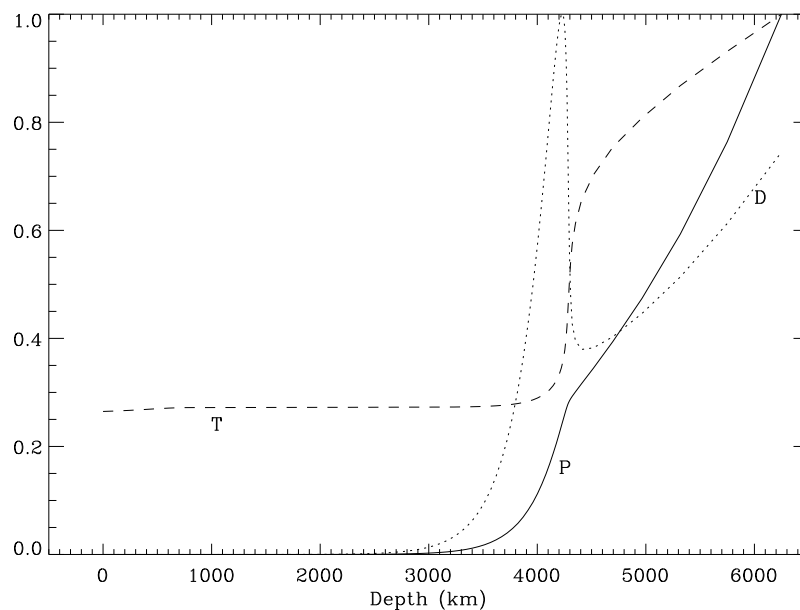## A.2   Atmospheric model of α Cir

In this section, I analyse an atmospheric model of α Cir supplied by Friedrich Kupka (private communication). Even though the model is not accurate due to the complexity of Ap star atmospheres, it can be used to test the feasibility of radial nodes situated in the observable atmosphere (see Chapters 5–6 for observational results on α Cir).

Figures A.4–A.6 show various quantities versus geometric depth in the atmospheric model. The continuum emission is formed at around a depth of 4200 km from the defined 'surface' of the star (Fig. A.5).

The distance between nodes of a standing wave is equal to $v/2f$, where v is the sound speed and f is the frequency of the pulsation (2442 μHz for α Cir). I numerically integrated $1/v$ with respect to the geometrical depth (D) in order to find the positions of the radial nodes in the atmosphere.

$$N(D) = 0.5 + 2f \int_0^D \frac{1}{v(D')} \, \mathrm{d}\, D' \tag{A.1}$$

where integer values of N represent nodes and the surface of the star is assumed to be an anti-node ($N = 0.5$). Figure A.7 shows the positions of 3 nodes in the atmospheric model, of which one is at a depth of about 3400 km and probably in the line-forming region of the atmosphere. Even though this model is not an accurate description of an Ap star atmosphere, it shows that the hypothesis of radial nodes situated in the observable atmosphere is reasonable.

Figure A.4 Pressure, density and temperature in the atmospheric model of α Cir (supplied by F. Kupka, private communication). Each line has been normalized by dividing by the maximum value in the plotted region ($P/76000$, $D/3.4 \times 10^{-8}$, $T/23300$ in *cgs* units). Note that there is a problem with the model, in that the density has a local maximum around 4200 km.
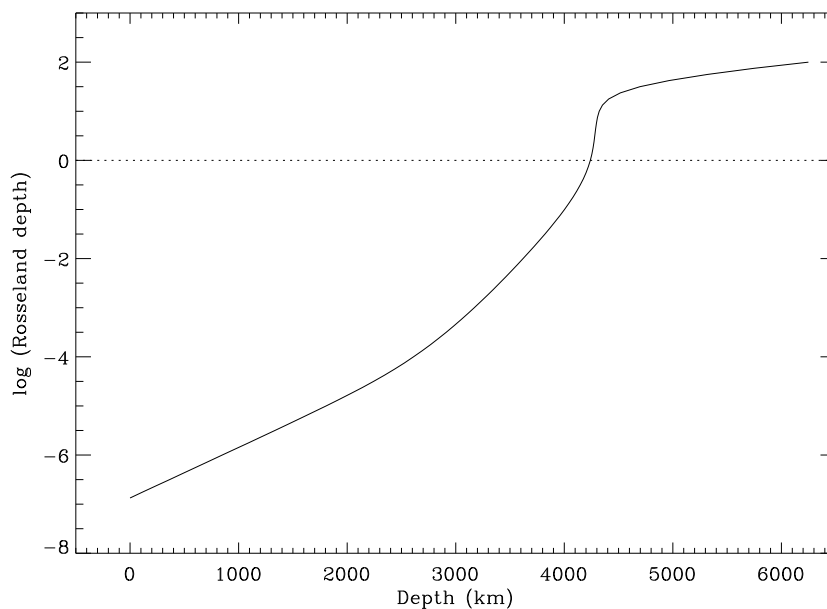
Figure A.5 Rosseland depth as a function of geometric depth in the atmospheric model. The observable region of the atmosphere is at geometric depths of less than 4300 km.
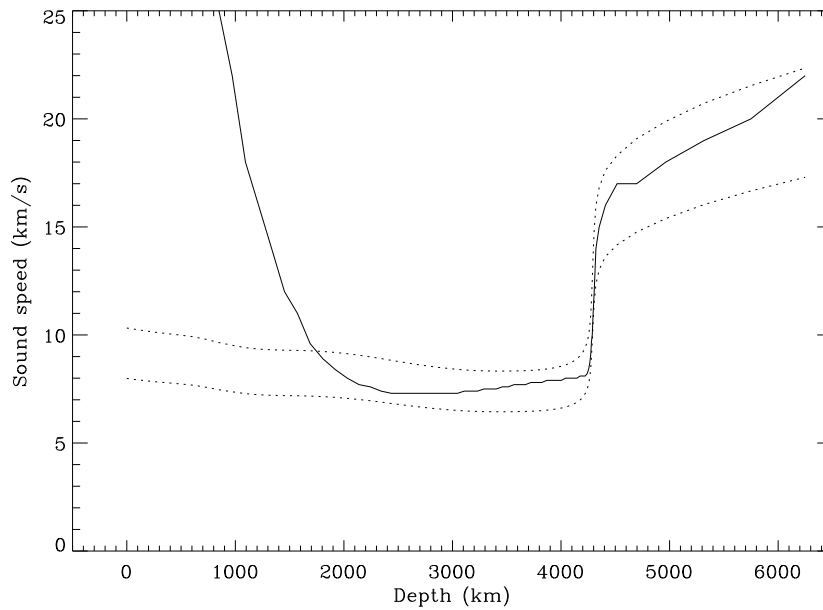
Figure A.6   Sound speed in the atmospheric model. The solid line is the calculated value in Kupka's model, while the dotted lines represent the sound speed from the adiabatic equation $v = \sqrt{\gamma P / D}$ with $\gamma = 1.0$ and 1.67.
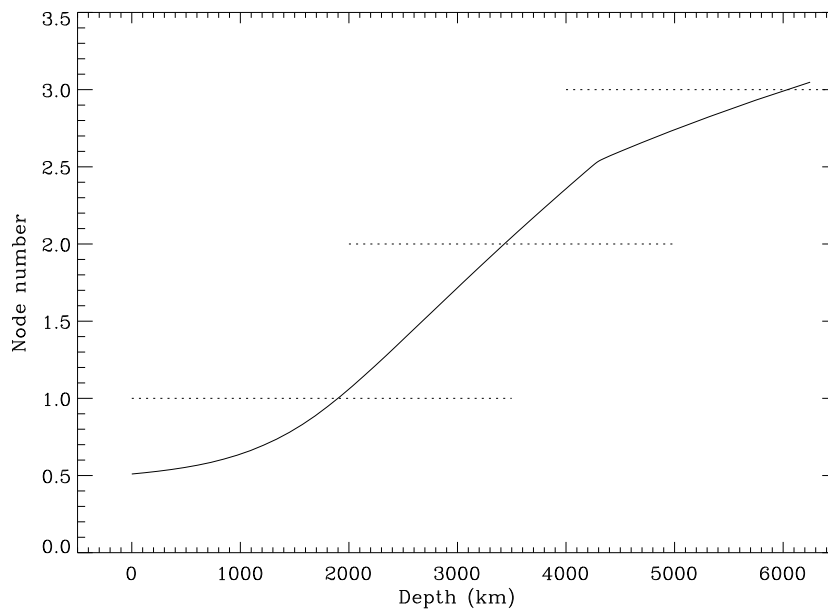
Figure A.7   Nodes in the atmospheric model. Integral numbers represent the node positions, with anti-nodes at the integer$+0.5$ values. The edge of the star is assumed to be an anti-node.

A.3 Variation of the width of Hα in α Cir

At the same time as measuring the bisector of the Hα line (Section 6.2.2), the width of the line at each height was measured. This is a similar analysis to measuring the intensity or equivalent-width changes. Measuring widths is a non-standard analysis but it has the advantage of isolating intensity changes at different heights in the Hα profile and the effect of the bisector variation is naturally removed from the measurements (see Chapters 6–7 for Hα profile variations in α Cir and HR 3831).

Fig. A.8 shows the amplitudes and phases of the principal mode as measured in variations in line width at different heights in the Hα profile (in α Cir). The phases of all the measurements lie between $-10°$ and $30°$, with the exception of section 20 (height 0.80–0.85), which is anomalous in both amplitude and phase. Since our phase reference point (t_0) coincides with maximum light (see Chapter 5), we conclude that the width of the Hα line is pulsating in phase with the luminosity. This is expected, since maximum width of the Hα line indicates maximum temperature in the stellar atmosphere.

The behaviour seen in Fig. A.8 can mostly be explained by changes in intensity in the line profile, which would affect the width by varying degrees, depending on the slope of the line profile. To quantify this, we have simulated a profile variation with an equivalent-width (EW) amplitude of 1000 ppm, where the change in intensity at each wavelength was chosen (somewhat arbitrarily) to be proportional to the depth of the absorption at that wavelength. The profile variation is shown greatly exaggerated in Fig. 6.6. The EW amplitude used in the simulation is same as the value predicted in Section 6.4.3. From the simulation, we measured the width amplitudes and compared it with our data (see dashed line in Fig. A.8). The agreement is good, although there are discrepancies near the core of the line and around a height of 0.75, where the width amplitude drops nearly to zero in the data but not in the simulation. Note this simulation is not based on model atmospheres but is only a description which fits the data reasonably well.
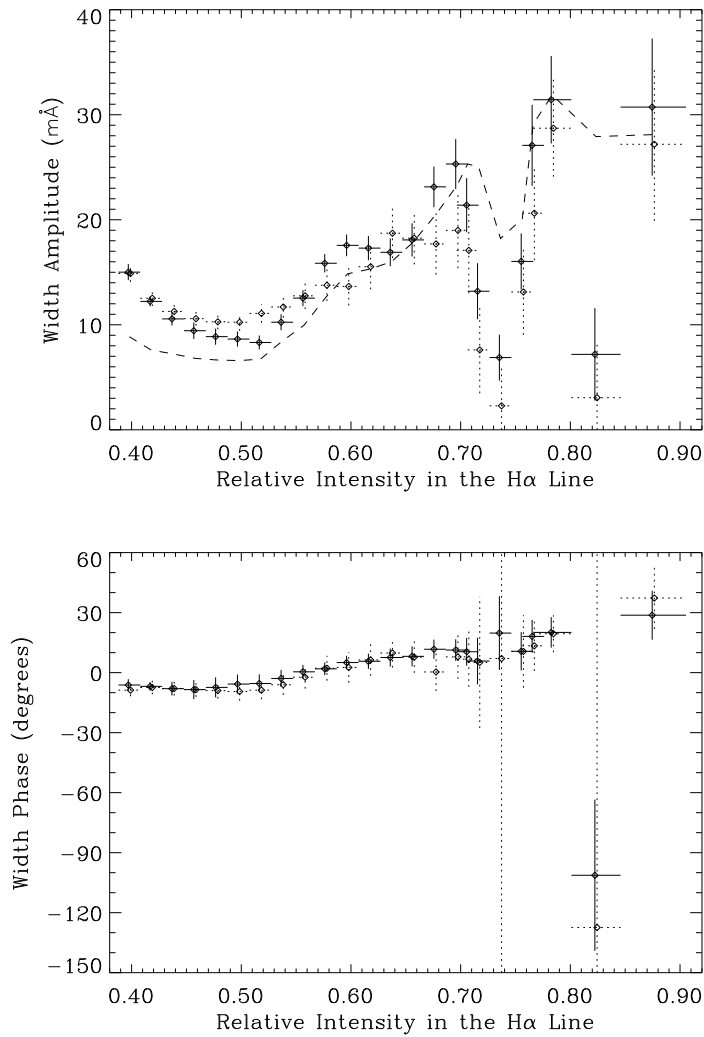
Figure A.8 Amplitudes and phases of the principal pulsation mode for the width at different heights in the Hα line (in α Cir). Points with solid lines represent the Stromlo data and points with dotted lines represent the La Silla data. For each measurement, the vertical line is an error-bar while the horizontal line shows the extent of the section in the Hα line. The dashed line shows the effect on the width amplitude of an oscillation with an EW amplitude of 1000 ppm.

Appendix B

B.1 Spectra of HR 3831

In March 1997, I observed HR 3831 using the coudé spectrograph on the 74-inch Telescope at Mt. Stromlo. During one week, 1400 spectra were obtained with a wavelength range of 6100–7100Å and with a resolution of about 1.5Å (see Chapter 7 for results based on these spectra).

The template spectrum of HR 3831 is shown in Figures B.1 and B.2. The S/N in this spectrum is about 1000 per pixel, though the continuum level is only accurate to about 0.01 between 6250Å and 6900Å and is less accurate outside this region.
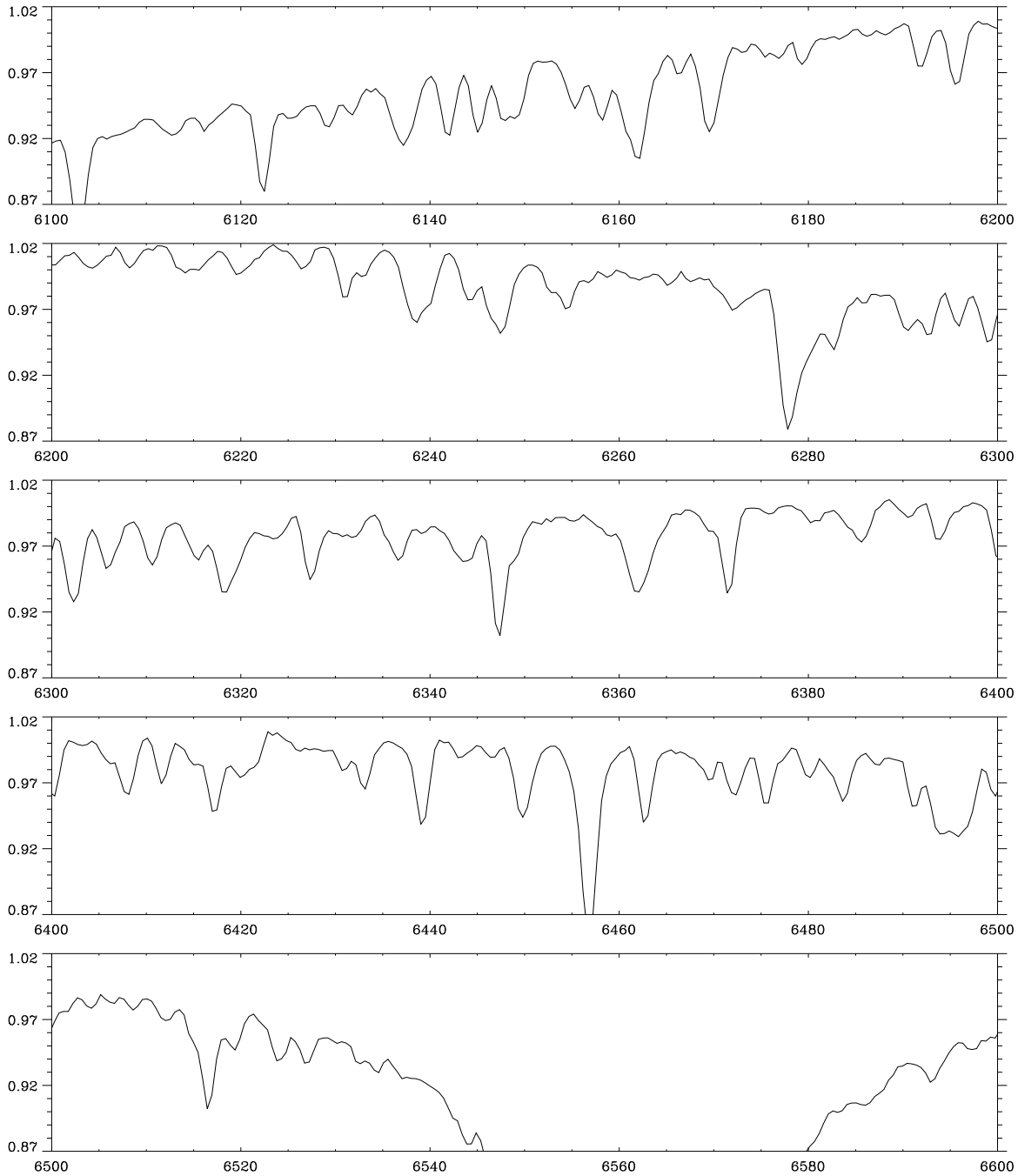
Figure B.1 Spectrum of HR 3831 from 6100 to 6600Å, taken with a medium resolution (~ 1.5Å) spectrograph at Mt. Stromlo. Note that the continuum fit is not accurate below 6250Å.
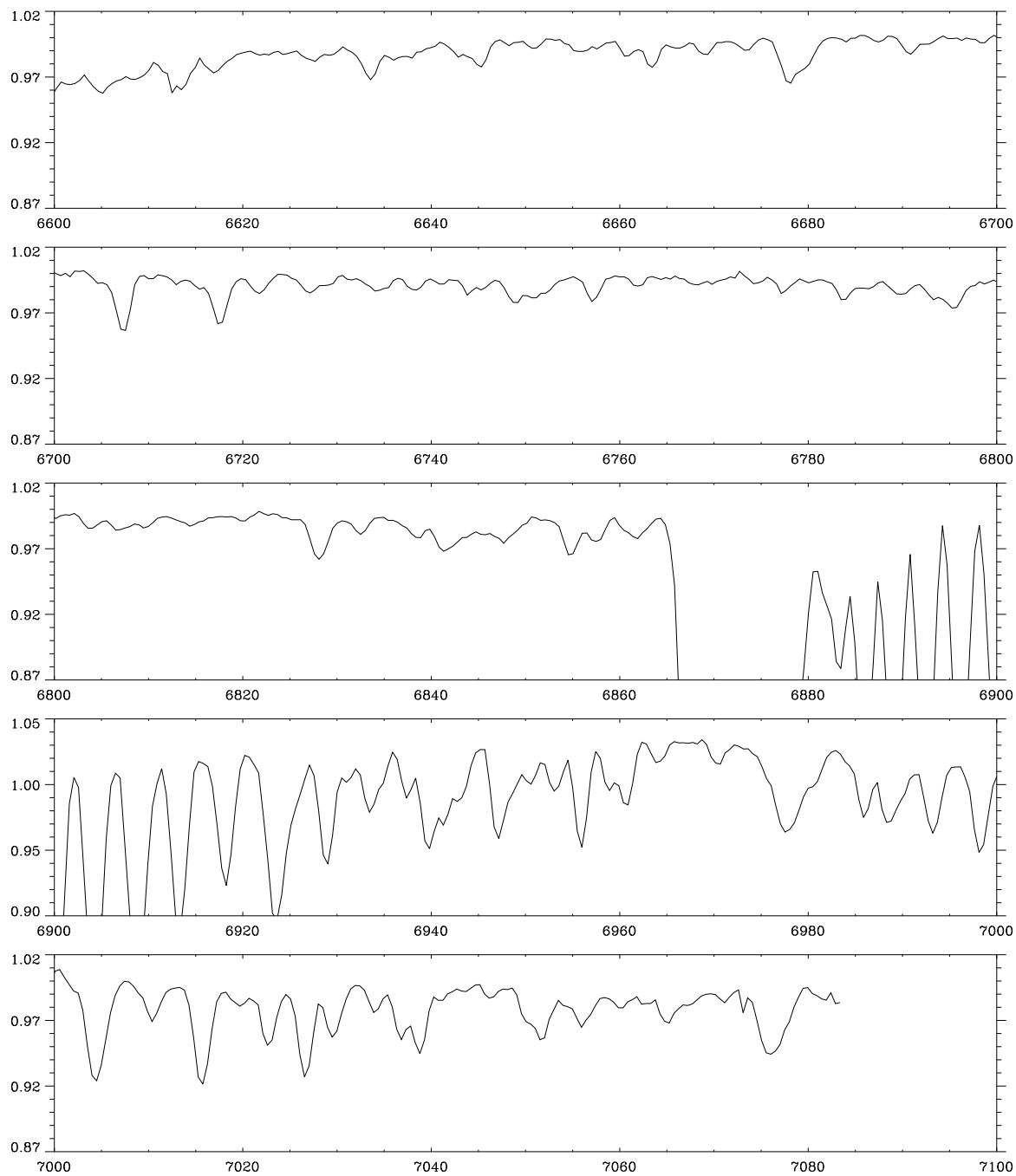
Figure B.2 Spectrum of HR 3831 from 6600 to 7100Å — continuation of Figure B.1. Note that the continuum fit is not accurate between 6900Å and 7000Å. The y-scale for this region is slightly shifted as a result.

B.2   Extra figures of rotational modulation in HR 3831

If oblique pulsator model is correct, HR 3831 pulsates in a dipole mode with an axis that is oblique to the rotation axis. Different aspects of the mode are seen as the star rotates and therefore, the measured amplitude and phase of the pulsation modulates with the rotation (see Chapter 7 for details).

Several observables were defined from the spectra of HR 3831. For each observable, a time series of measurements was analysed to determine the amplitudes and phases of the frequency triplet. Additionally, the data for each observable were divided into 20 separate time periods, and the amplitude and phase of the pulsation were measured for each period (see Section 7.3 for details).

Plots of the modulation in the amplitude and phase of various observables are shown in Figures B.3–B.18, 7.4, 7.5 and 7.8. The figures show the amplitude and phase of the central frequency as a function of rotation phase. The squares represent the data divided into 20 separate time periods between 0.5 and 3.6 hours long. The vertical lines are error bars, while the horizontal lines show the length of the time period. The dashed line represents a fit based on the measurement of the frequency triplet from the complete time series, and the dotted line represents a fit which is scaled and phase shifted from the photometric frequency triplet (Table 7.2). Note that the data are plotted twice.

Figs. B.3–B.12, 7.5 and 7.8 show observables based on the cross-correlation measurements of various wavelength bands. Figs. B.13–B.16 show bisector velocity and width measurements of the Hα line. Figs. B.17–B.18 and 7.4 show direct intensity measurements of the Hα core and an R_{cw} intensity ratio measurement.
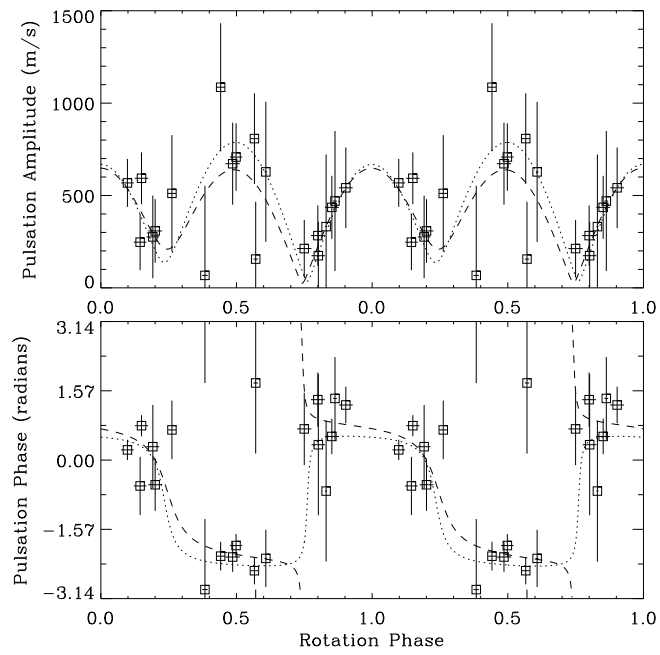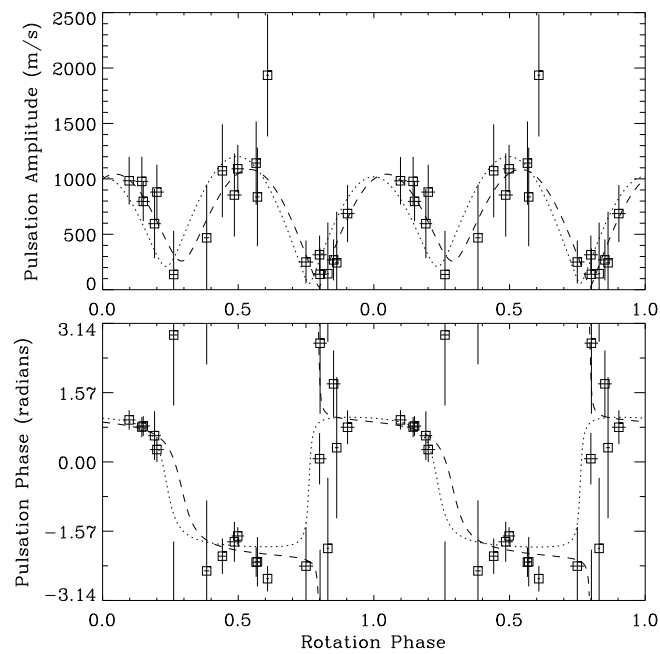
Figure B.3 Velocity amplitude and phase of band no. 13
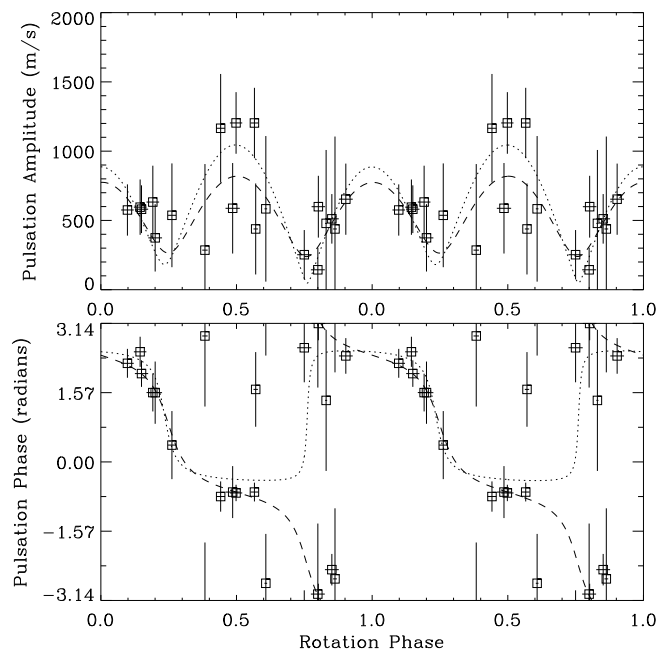
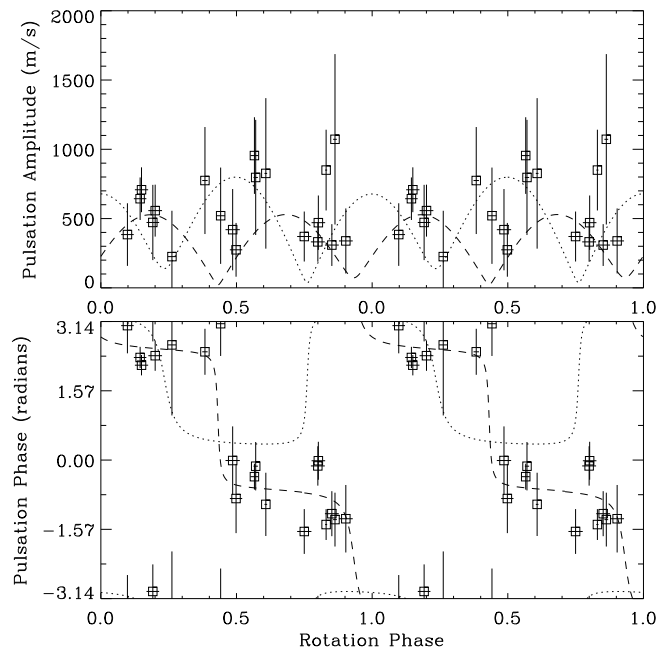**Figure B.4** Velocity amplitude and phase of band no. 14
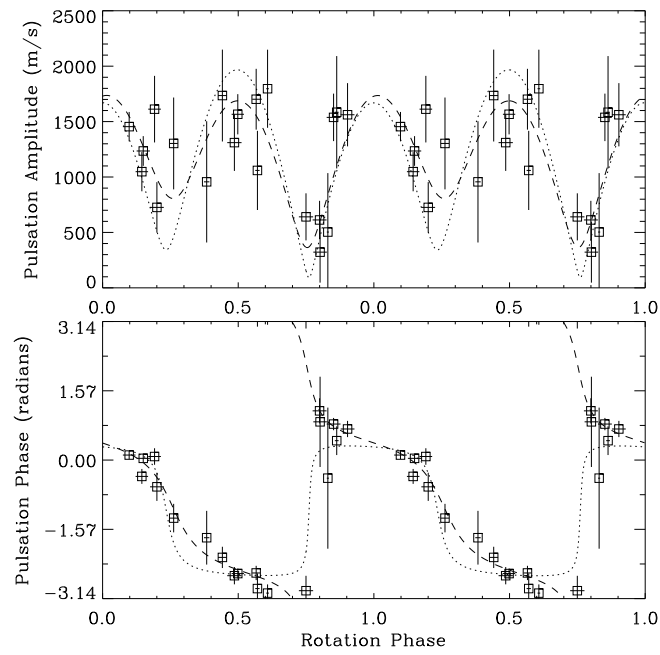
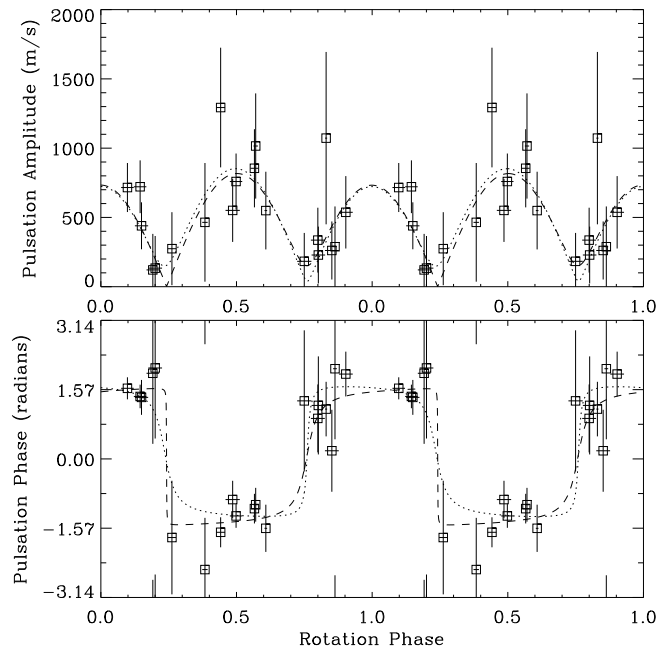**Figure B.5**   Velocity amplitude and phase of band no. 33

Figure B.6   Velocity amplitude and phase of band no. 42
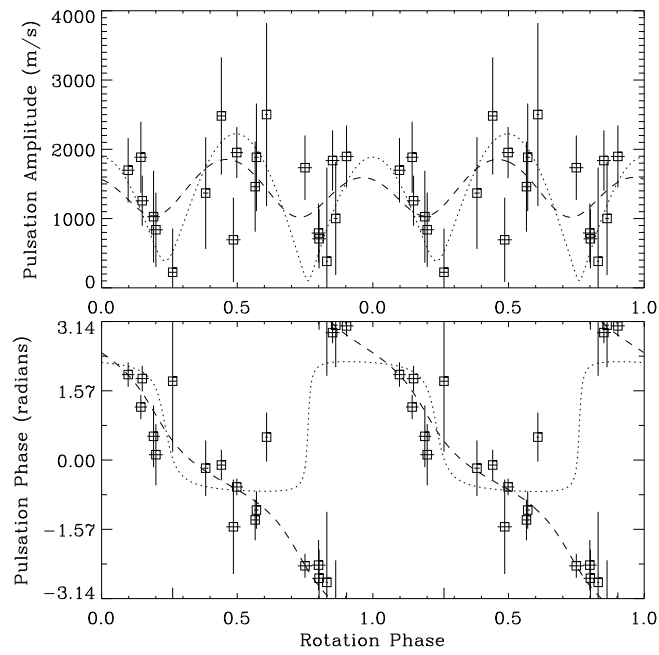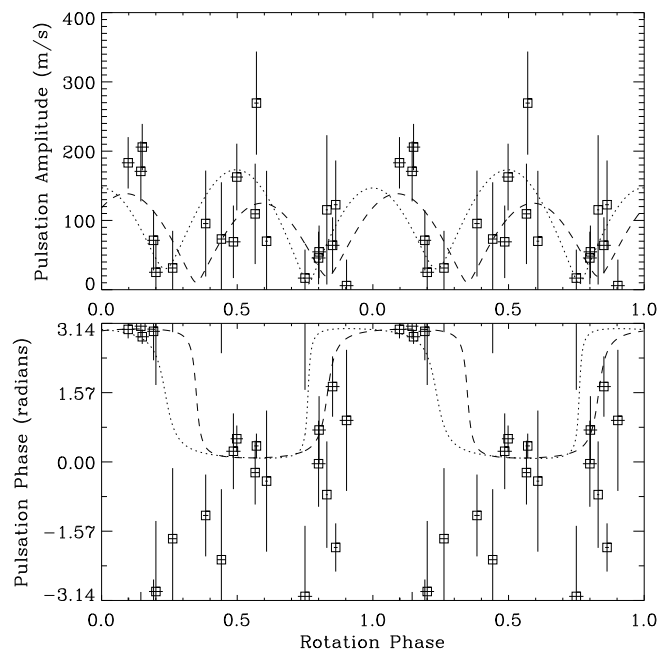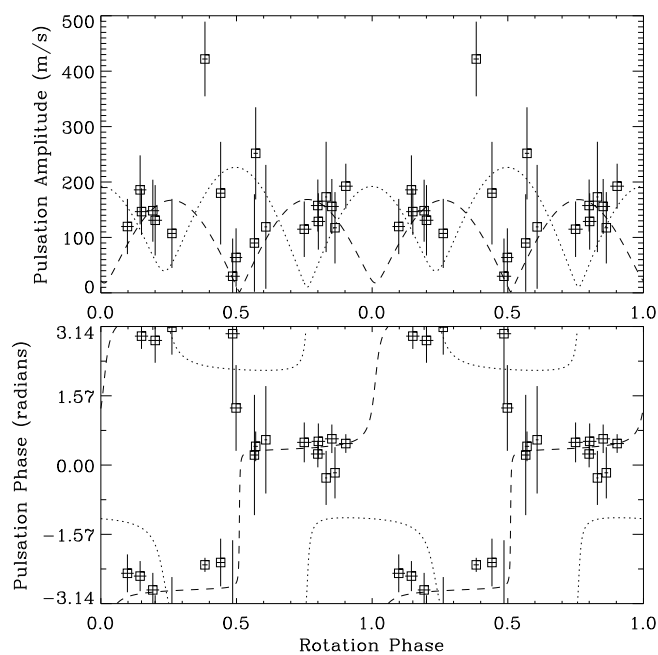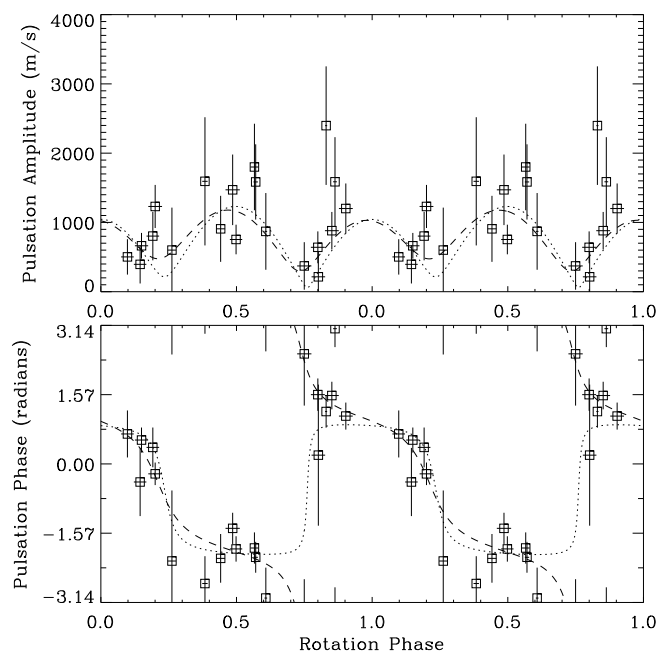
Figure B.7 Velocity amplitude and phase of band no. 48

Figure B.8 Velocity amplitude and phase of band no. 54

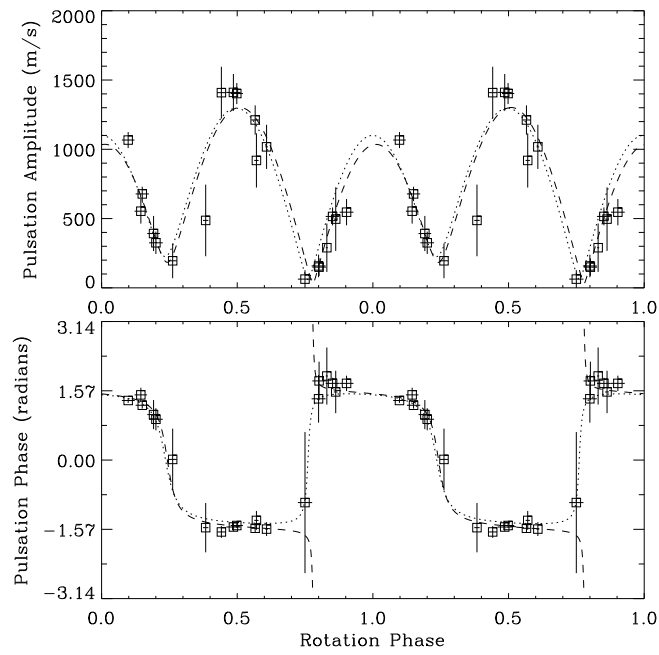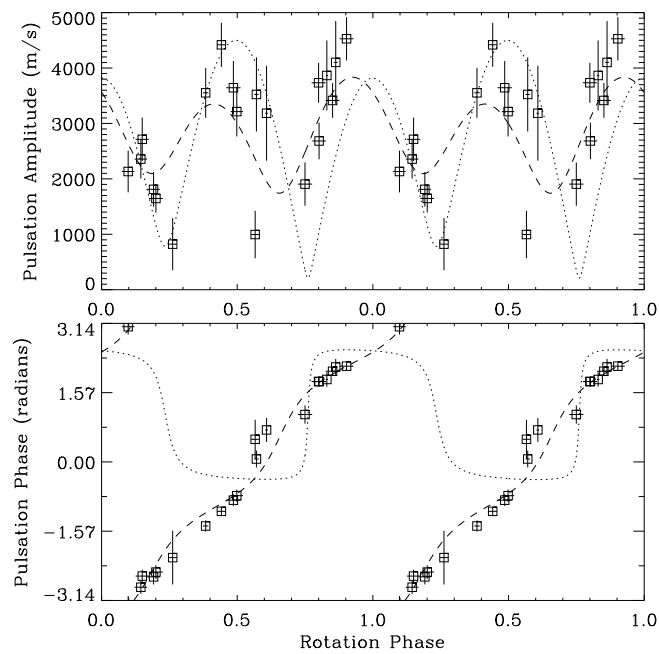**Figure B.9**   Velocity amplitude and phase of band no. 58

Figure B.10   Velocity amplitude and phase of band no. 81

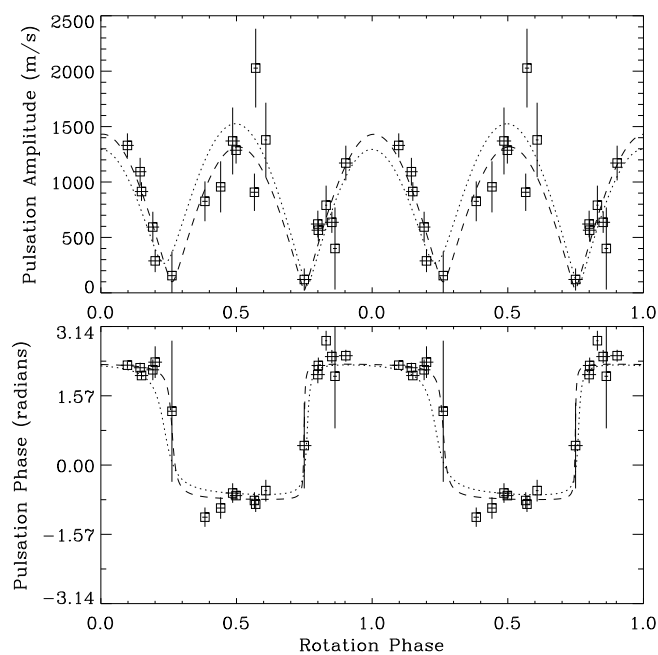**Figure B.11**   Velocity amplitude and phase of band no. 82

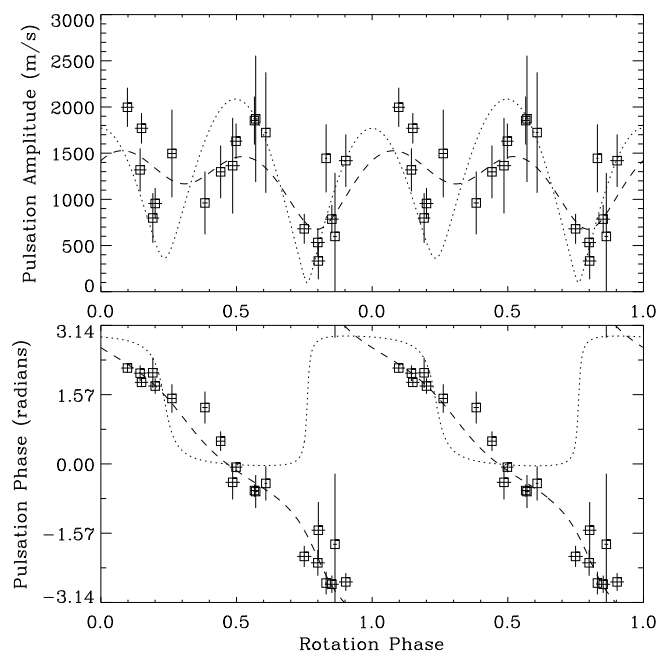**Figure B.12**   Velocity amplitude and phase of band no. 90

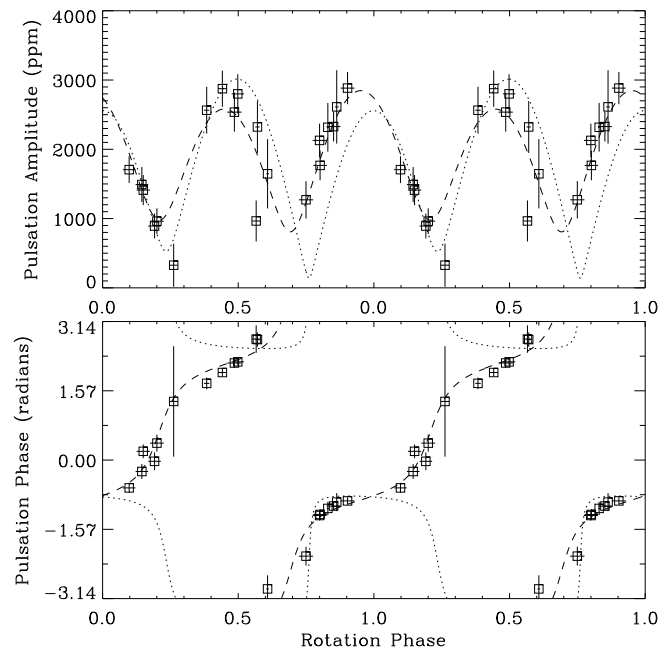**Figure B.13**   Velocity amplitude and phase of the Hα bisector at height 0.40

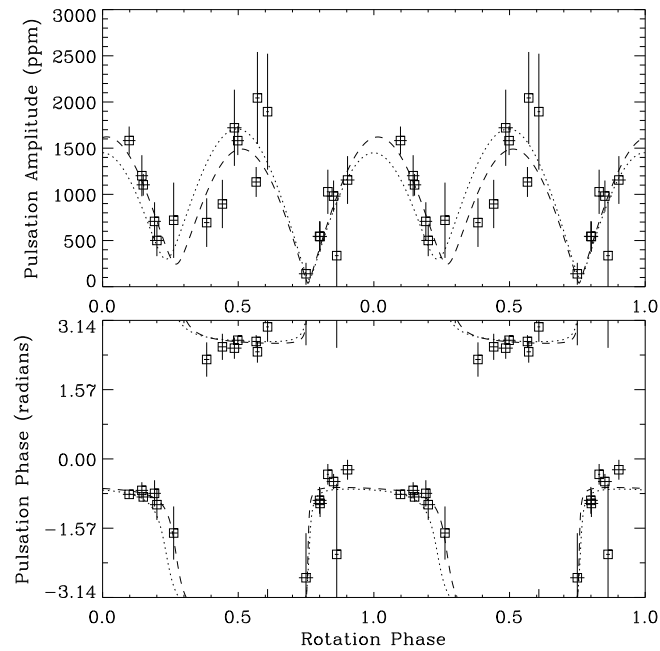**Figure B.14**   Width amplitude and phase of the Hα line at height 0.36

Figure B.15 Width amplitude and phase of the Hα line at height 0.42

Figure B.16 Width amplitude and phase of the Hα line at height 0.53

Figure B.17   Intensity amplitude and phase of the Hα core, using a filter with FWHM∼1.0Å

Figure B.18   Intensity amplitude and phase of the Hα core, using a filter with FWHM∼5.9Å